Sensors and Materials, Vol. 37, No. 1 (2025) 1–11
MYU Tokyo

S & M 3887

GaN–MoS_2 Composite Nanowires Grown on Graphite Paper as Battery-type Electrode Materials

Ting Wang,[1,2] Shang-Chao Hung,[3] and Wein-Duo Yang[4*]

[1]Department of Artificial Intelligent Engineering, Fuzhou Polytechnic, Fuzhou 350108, China
[2]School of Materials Science and Engineering, South China University of Technology, Guangzhou 510641, China
[3]School of Mathematics and Information Engineering, Longyan University, Longyan 364012, China
[4]Department of Chemical and Materials Engineering, National Kaohsiung University of Science and Technology, Kaohsiung 80778, Taiwan,

(Received October 8, 2024; accepted January 9, 2025)

Keywords: GaN–MoS_2 composite nanowire, chemical vapor deposition, battery-type electrode materials, supercapacitor

Supercapacitors have become promising energy storage devices owing to their high power density and fast charging capability. Herein, we synthesized GaN nanowires coated with MoS_2 nanosheets on graphite paper by chemical vapor deposition and explored their electrochemical properties. Both GaN nanowire and MoS_2-coated GaN composite nanowire electrodes exhibit Faradaic behaviors from redox reactions. The MoS_2-coated GaN composite nanowire electrodes show enhanced electrochemical activities with a capacity of 173.4 mC cm^{-2} at 1 mA cm^{-2}. Thin MoS_2 nanosheets are quasi-perpendicularly grown onto the GaN nanowire surface, which prevents their aggregation. The coupling of MoS_2 nanosheets with GaN nanowire enables a high surface area and provides channels to facilitate ion diffusion. In this work, we demonstrate the GaN–MoS_2 composite nanowires as potential flexible battery-type electrode materials in wearable electronics and sustainable energy applications.

1. Introduction

Two major challenges, energy crisis and environmental issues, make the development of efficient, clean, and sustainable energy storage an urgent task. Supercapacitors (SCs), which are new energy storage devices, have a number of advantages, such as high power density, fast charging and discharging capabilities, and long cycle life.(1) SCs rely on the physicochemical changes that occur at the active electrode materials and electrolyte interface. Hence, the development of high-performance electrode materials has become one of the research hotspots.(2) It is important to judge whether the nanomaterial is battery-like or capacitor-like, as well as to determine electrical energy storage mechanisms.(3) The charge storage of capacitor-like electrode materials comes from two components: the electrical double-layer capacitance (EDLC), which builds up electrical charge at the electrode/electrolyte interface, and the pseudo-capacitance that originates from the surface Faradaic redox reactions at the interface at certain potentials.(4) The

*Corresponding author: e-mail: ywd@nkust.edu.tw
https://doi.org/10.18494/SAM5179

ISSN 0914-4935

capacity of battery-like electrode materials predominantly depends on Faradaic electron transfer to metal centers by the intercalation of charge-compensating ions.[5] Recently, a number of active materials with superior performance have been developed for SC electrodes, including carbon-based materials, metal oxides, and conductive polymers.[6–8]

In addition to the above most studied materials, metal nitrides (such as TiN,[9] Nb_4N_5,[10] and CrN[11]) have attracted extensive attention as electrode materials for SCs because of their excellent conductivity and high specific capacitance. GaN, a representative of wide-band-gap semiconductors, is considered a potential candidate for electrode materials of SCs owing to its high electron mobility, good electrochemical reversibility, thermal stability, and so forth.[12–15] The large aspect ratio and strong mechanical deformation resistance of nanostructured materials increase the contact area between the electrode and the electrolyte, shortening the transmission path of electrons and ions, which is beneficial to the capacitance performance of the electrode.[16] Symmetric SCs based on single-crystal GaN mesoporous membrane and GaN nanowire (NW) electrodes have been explored,[13,14] and GaN-based electrode materials are developed and upgraded for harsh environments.[17,18] Moreover, MoS_2 has been recognized as a promising electrode for SCs because MoS_2-based electrodes show a higher intrinsic ionic conductivity than metal oxides and fast electron transportation.[19–23] 2D layered MoS_2 nanosheets (NSs) have a large number of unsaturated chemical bonds, which are active sites for charge transfer and can enhance the controlled transport of ions and electrons at small diffusion scales, thereby improving the performance of SCs. However, the insertion/extraction of ions during charging and discharging will result in the structure deformation and collapse of the MoS_2-based electrode materials.[24] Thus, the growth of MoS_2 NSs on the surface of GaN NWs may be an effective method to eliminate the shortcoming. The GaN NWs employed as scaffolds are more resistant to mechanical deformation. Therefore, the synergistic effects of graphite paper (GP), GaN, and GaN–MoS_2 composite NW electrodes may effectively improve the performance of flexible SCs.

In this work, flexible electrodes of GaN–MoS_2 composite NWs grown on GP were designed and used. Both GaN NWs and MoS_2 NSs were synthesized by chemical vapor deposition. The GaN–MoS_2 composite NWs are composed of thin MoS_2 NSs perpendicular to GaN NWs. The electrochemical performance of the composites was studied in detail. Benefiting from the large surface-to-volume ratio and the high conductivity of the flexible GP substrate, the GaN–MoS_2 composite NWs exhibited enhanced electrochemical activities.

2. Experiment

2.1 Synthesis of GaN–MoS_2 composite NWs

GaN NWs were fabricated by chemical vapor deposition in a horizontal tubular furnace, as described in our previous report.[25] In brief, graphite paper (GP) coated with a thin Au layer (~8 nm) was used as the substrate. Ga_2O_3 powder (Macklin, 99.99%) and NH_3 (99.999%) were precursors. The growth temperature and the flow rate of the gas mixture (Ar:NH_3 = 1:2) were 1050 °C and 300 sccm, respectively. For the growth of MoS_2, a layer of Mo was coated on GaN NWs by DC magnetron sputtering, followed by vulcanization in sulfur atmosphere for 15

min.[26] The growth temperatures of MoS_2 were 400, 450, 500, and 550 °C, and the corresponding samples obtained are denoted as GM-400, GM-450, GM-500, and GM-550, respectively.

2.2 Characterization of materials

The morphology of GaN and GaN–MoS_2 composite NWs was studied by field emission scanning electron microscopy (FESEM, FEI Nova NanoSEM 430). TEM (JEOL JEM-2100F) with energy-dispersive X-ray analysis (EDX) (Oxford instruments) was carried out to examine the crystalline nature of GaN and GaN/MoS_2 NWs. The crystal structure was characterized by X-ray diffraction (XRD, PANalytical X' pert PRO, Cu Kα, λ = 1.540598 Å). Micro-Raman spectra were characterized at room temperature on a Renishaw system equipped with a microscope operated in a back-scattering configuration (inVia-58P056 laser Raman spectrometer) and excited with a 532 nm laser. Room-temperature photoluminescence (PL) spectra of GaN and GaN–MoS_2 composite NWs were measured with an Edinburgh FLS 920 luminescence spectrometer (Xe lamp, the excitation wavelength was 316 nm). X-ray photoelectron spectroscopy (XPS, Kratos Axis Ultra DLD) spectra were obtained with a monochromatic Al Kα source and a 700 × 300 μm^2 spot size.

2.3 Electrochemical characterization

The electrochemical properties of the composites were characterized at room temperature by galvanostatic charge/discharge (GCD) and cyclic voltammetry (CV) techniques using an electrochemical workstation (France, Bio-Logic, VMP3, SP-150). The data were obtained in a three-electrode system: a platinum sheet (1.5 × 1.5 cm^2) was used as the counter electrode, a saturated calomel electrode (SCE) as the reference electrode, 1 mol L^{-1} H_2SO_4 aqueous solution as the electrolyte, and the GaN–MoS_2 composite NWs on GP (1 × 1 cm^2) as the working electrode. For comparison, GaN NWs on GP were also applied as the active material. CV and GCD curves were collected at −0.2 to 0.9 V by varying the scan rate from 5 to 100 mV s^{-1} and the current density from 1 to 20 mA cm^{-2}.

The capacity (C, mC cm^{-2}) of the electrode material can be fundamentally characterized by the three-electrode system and calculated from the GCD curves. The C derived from the GCD curves was calculated as

$$C = \frac{i\Delta t}{s}, \tag{1}$$

where s is the area of the active material on the working electrode (cm^2), i is the constant discharge current (mA), and Δt is the discharge time (*s*).

3. Results and Discussion

The GaN–MoS_2 composite NWs were grown on GP as described in the experiment section. Figures 1(a)–1(d) show the SEM images of GaN–MoS_2 composite NW samples of GM-400, GM-450, GM-500, and GM-550, respectively. The insets are the corresponding high-resolution SEM images of a single NW. The average diameter and length of these NWs are about 200 nm and several micrometers, respectively. As the growth temperature increases from 400 to 500 ℃, the amount and size of MoS_2 NSs increase accordingly and reach maximum at 500 ℃. Further increasing the growth temperature leads to the decreases in the amount and size of MoS_2 NSs, which can be clearly observed from the inset SEM images.

The more detailed microstructure of the composite NWs was analyzed by TEM. Figure 2(a) is a TEM image of a typical GaN NW, showing a corrugated shape. Figures 2(b) and 2(d) are TEM images of GM-450 and GM-500 NWs, respectively. MoS_2 NSs are grown perpendicularly to the surface of GaN NWs. The amount and dimension of MoS_2 NSs are greater in GM-500 than in GM-450. Figures 2(c) and 2(e) are high-resolution TEM (HRTEM) images of GM-450 and GM-500 corresponding to the red rectangle areas in Figs. 2(b) and 2(d). The lattice fringe spacings of 0.26 and 0.62 nm are consistent with the interspacing of hexagonal wurtzite GaN (002) planes and hexagonal wurtzite MoS_2 (002) planes, respectively. Figure 2(f) shows the selected area electron diffraction (SAED) pattern of GM-500, revealing the single crystalline nature of the GaN NW. The diffraction rings belong to MoS_2, and the smallest diffraction ring corresponds to the (100) planes. Figure 2(g) is the high-angle annular dark-field (HAADF)

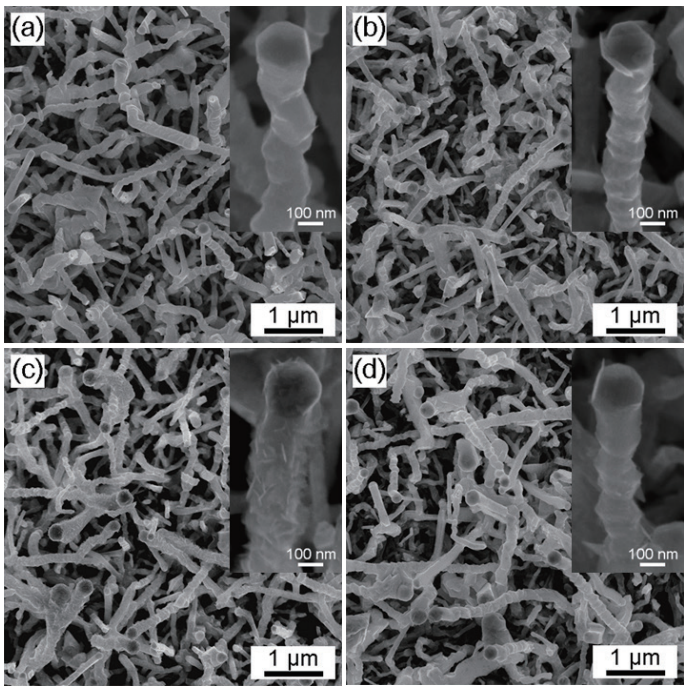

Fig. 1. FESEM images of (a) GM-400, (b) GM-450, (c) GM-500, and (d) GM-550. The insets are corresponding enlarged views of a single NW.

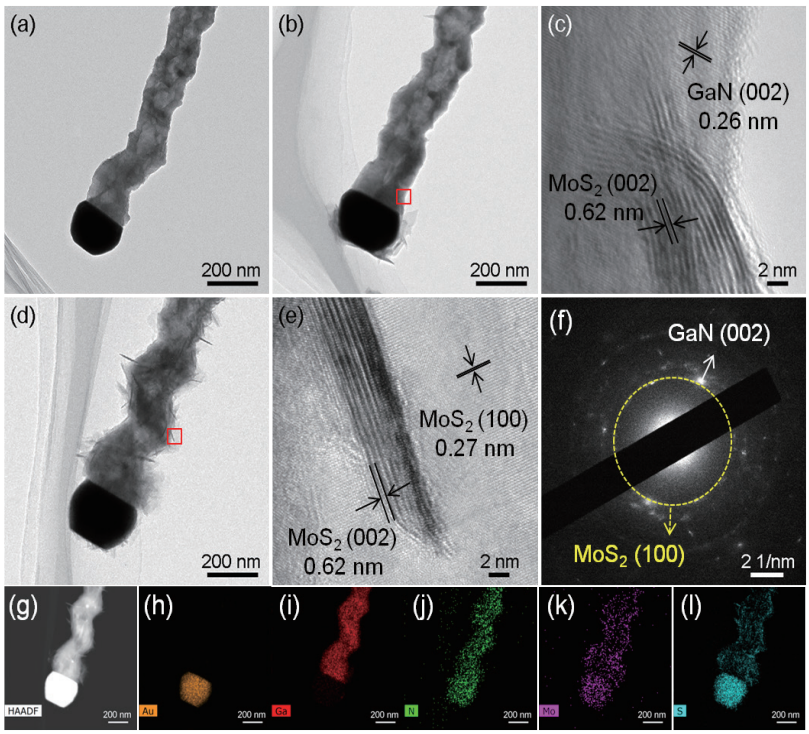

Fig. 2. (Color online) (a) TEM image of a single GaN NW; (b) TEM image of a single GaN–MoS_2 composite NW of GM-450; (c) HRTEM image of GM-450 in the red rectangle shown in (b); (d) TEM image of a single GaN–MoS2 composite NW of GM-500; (e) HRTEM image of GM-500 in the red rectangle shown in (d); (f) corresponding SAED pattern of the middle region of GM-500; (g) HAADF image of GM-500; (h)–(l) element mappings of Au, Ga, N, Mo, and S, respectively.

image of the GM-500 NW. Figures 2(h)–2(l) are the element mappings of Au, Ga, N, Mo, and S, respectively. The Ga and N elements are uniformly distributed throughout the GaN NW, whereas the Mo and S elements are mainly distributed around the NW, demonstrating the formation of the GaN–MoS_2 composite NW. Au is concentrated at the top of the NW, suggesting the vapor-liquid-solid growth mechanism of GaN NWs.

The XRD spectra of the GaN and GaN–MoS_2 composite NWs are shown in Fig. 3. The diffraction peaks centered at 32.4, 34.6, and 36.9° are indexed to the hexagonal wurzite GaN (100), (002), and (101) planes (JCPDS: 50-0792), respectively. The peaks marked with solid dots are the signals from the GP substrate (JCPDS: 75-2078), and those marked with hollow dots are diffraction from Au (JCPDS: 04-0784). No MoS_2 related diffraction detected may be due to the relatively small amount of MoS_2.

Figure 4 depicts the room-temperature PL and Raman spectra of GaN and GaN–MoS_2 composite NWs. All samples exhibit a strong UV emission centered at 366 nm accompanied by a weak yellow luminescence, which is attributed to the near-band emission (NBE) and surface defect-related emission (such as V_{Ga} vacancy) of GaN.[25] Although there is no PL emission from MoS_2 NSs, it matches well with the characteristics of multilayer MoS_2.[26] The Raman spectra of the samples are presented in Fig. 4(b). Hexagonal GaN has a wurtzite structure and belongs to the C (P63mc) space group. According to the results of the factor group analysis at the Γ point,

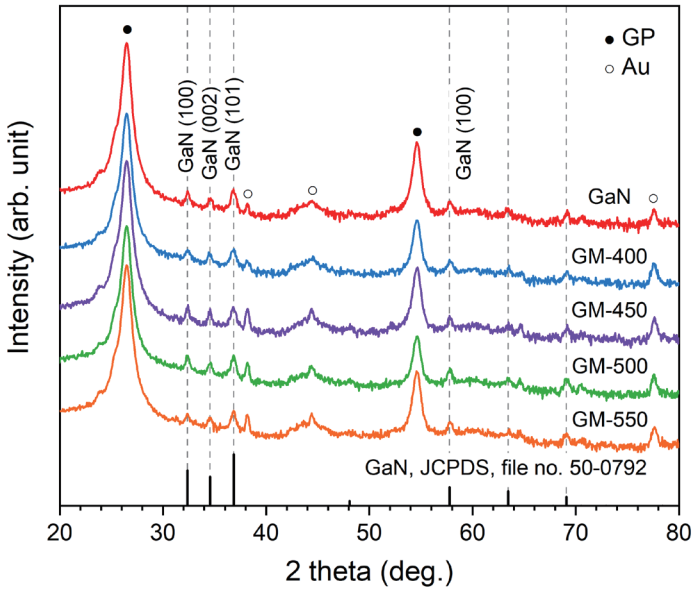

Fig. 3. (Color online) XRD patterns of GaN and GaN–MoS_2 composite NWs of GM-400, GM-450, GM-500, and GM-550.

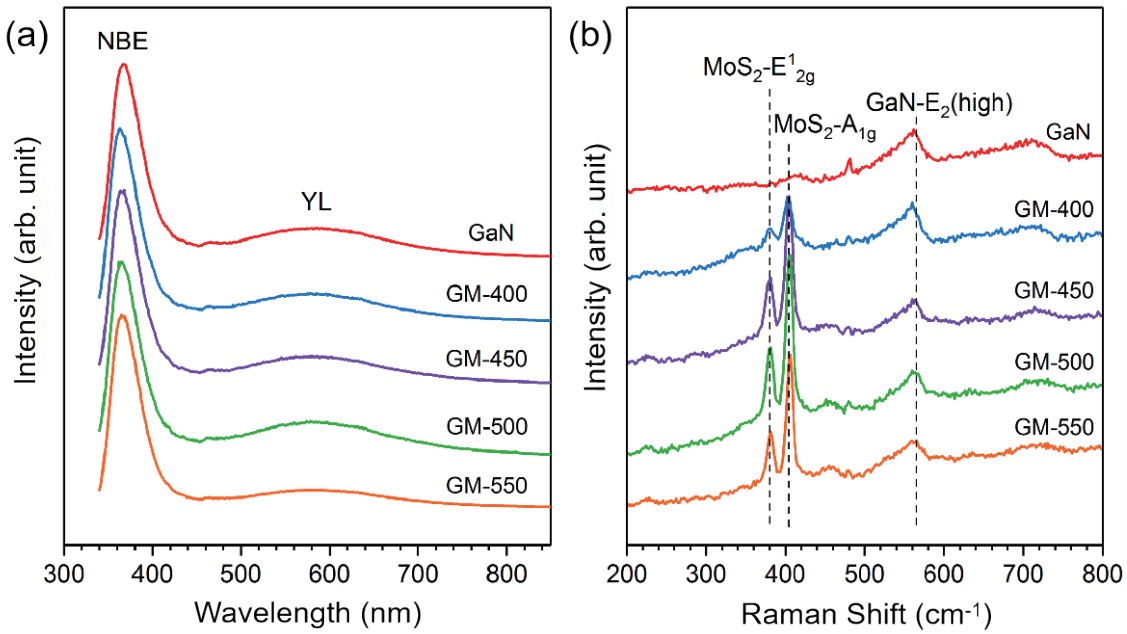

Fig. 4. (Color online) (a) PL and (b) Raman spectra of GaN and GaN–MoS_2 composite NWs of GM-400, GM-450, GM-500, and GM-550.

six first-order Raman optical modes, A_1(TO), A_1(LO), E_1(TO), E_1(LO), E_2(high), and E_2(low), are active.[27] The peak at 565 cm^{-1} can be identified to be the GaN-E_2(high) phonon mode, which is characteristic of the hexagonal GaN crystal.[28] The peaks at 380 and 404 cm^{-1} are the typical first-order Raman active modes of MoS_2-E^1_{2g} of the in-plane vibration of molybdenum and sulfur atoms and the MoS_2-A_{1g} mode of the out-of-plane vibration of sulfur atoms,

respectively. The frequency difference between the E^1_{2g} and A_{1g} modes of all the samples is about 24 cm^{-1}, which indicates that the MoS_2 NSs are multiple layers.[29] Thus, the growth temperature of MoS_2 only shows an effect on the dimension and amount of MoS_2 NSs attached to the surface of the GaN NWs.

To evaluate the electrochemical activity of GaN and GaN–MoS_2 composite NWs, a conventional three-electrode system was utilized for electrochemical measurement. The GaN and GaN–MoS_2 composite NWs on GP were used directly as flexible working electrodes. GM-450 and GM-500 were examined and compared. Figure 5(a) shows the CV curves measured

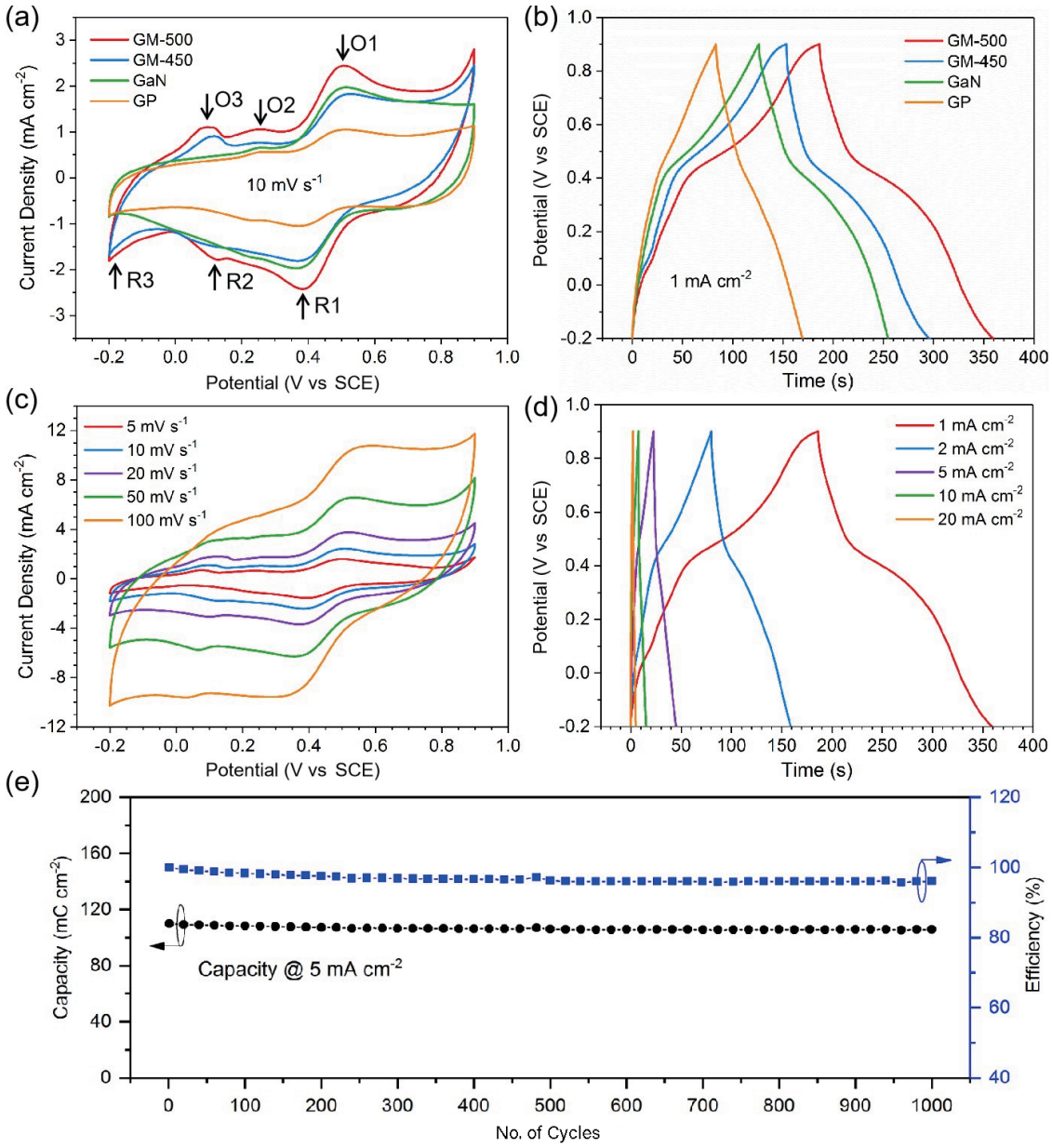

Fig. 5. (Color online) (a) CV curves of GP, GaN, GM-450, and GM-500 at a scan rate of 10 mV s^{-1}; (b) GCD profiles of GP, GaN, GM-450, and GM-500 at a current density of 1 mA cm^{-2}; (c) CV curves of the GM-500 electrode at a scan rate of 5 to 100 mV s^{-1}; (d) GCD profiles of the GM-500 electrode with current densities ranging from 1 to 20 mA cm^{-2}; (e) GCD cycling performance at a current density of 5 mA cm^{-2}.

from the samples in a voltage window of −0.2–0.9 V at a scan rate of 10 mV s^{-1}. The CV profile of the GP substrate is also provided for comparison. A quasi-rectangular and symmetric shape of the CV curve can be observed from the GP substrate electrode. As for the GaN NW electrode, two peaks were observed from the CV curve and marked by O1 and R1. In comparison, the GaN–MoS_2 composite electrodes of GM-450 and GM-500 exhibited more distinct peaks in the CV curves, as marked by O2/R2 and O3/R3. The appearance of redox peaks in CV curves of GaN and GaN–MoS_2 composite electrodes indicates typical surface Faradaic redox reactions. Figure 5(b) shows the GCD results of the samples at a current density of 1 mA cm^{-2}. The charge/discharge curve of the bare GP electrode shows a small charge/discharge plateau, indicating its intercalation pseudocapacitor characteristic, which is consistent with the CV curve. There appears a flat discharge plateau in the GCD curves of GaN and GaN–MoS_2 composite electrodes, which should be the contribution of Faradaic electron transfer. Moreover, the GCD curves of GaN–MoS_2 composite electrodes exhibit a longer discharging time than those of GaN electrodes, demonstrating an increased capacitance of the former. The enlarged capacity is mainly due to the increase in the number of active sites rendered by MoS_2 NSs. The C values of GaN–MoS_2 composite electrodes are greater than those of GaN electrodes in common. The maximum capacity of the GaN–MoS_2 composite electrode GM-500 reaches 173.4 mC cm^{-2} at 1 mA cm^{-2}, which is superior to that of the GaN electrode of 128.8 mC cm^{-2}, suggesting the enhanced capacity of the GaN–MoS_2 composite electrode. Figure 5(c) shows the detailed CV curves of GM-500 for scan rates of 5, 10, 20, 50, and 100 mV s^{-1}, showing nonlinear shapes with clear redox peaks. Figure 5(d) presents the GCD curves of the GM-500 electrode at current densities ranging from 1 to 20 mA cm^{-2}. The GaN–MoS_2 composite electrode of GM-500 exhibits excellent capacities of 173.4, 158.3, 112.7, 74.8, and 49.6 mC cm^{-2} at current densities of 1, 2, 5, 10, and 20 mA cm^{-2}, respectively. As the current density increases, the capacity exhibits a small decrease, indicating a fast charge/discharge capability.

The cycling performance of the GM-500 electrode is depicted in Fig. 5(e). The specific capacity of GM-500 at 5 mA cm^{-2} exhibits a slight reduction from 110.1 to 105.8 mC cm^{-2} after 1000 charge/discharge cycles, which shows cycling stability and retains ≈96% of its initial specific capacitance.

To investigate the mechanism of the GaN–MoS_2 composite electrode, the XPS characterization of the GM-500 electrode material was performed. Figure 6 shows the XPS core level spectra of Ga 3d, N 1s, Mo 3d, and S 2p. As shown in Fig. 6(a) of the Ga 3d spectrum, two peaks located at 20.9 and 20.2 eV are assigned to the Ga-N and Ga-N-O bonds, respectively.[30] As for the N 1s peak in Fig. 6(b), it can be deconvoluted into the contributions of the Ga-N bond (397.8 eV), Ga-N-O bond (396.3 eV), and Auger Ga peaks (395.3 and 394.2 eV).[31,32] The oxynitride layer on the surface of the GaN NWs is likely to be the origin of its capacity.[10,33–35] With H_2SO_4 aqueous solution as the electrolyte, an equilibrium reaction can be expressed as[13]

$$Ga_{x+2y/3}N_xO_y + 2zH^+ + ze^- \leftrightarrow Ga_{x+(2y-z)/3}N_xO_{y-z} + zH_2O\,, \tag{2}$$

where $Ga_{x+2y/3}N_xO_y$ and $Ga_{x+(2y-z)/3}N_xO_{y-z}$ represent the metal oxynitride active layer; x, y, and z are stoichiometric ratios; the reaction to the right represents the charging process, and

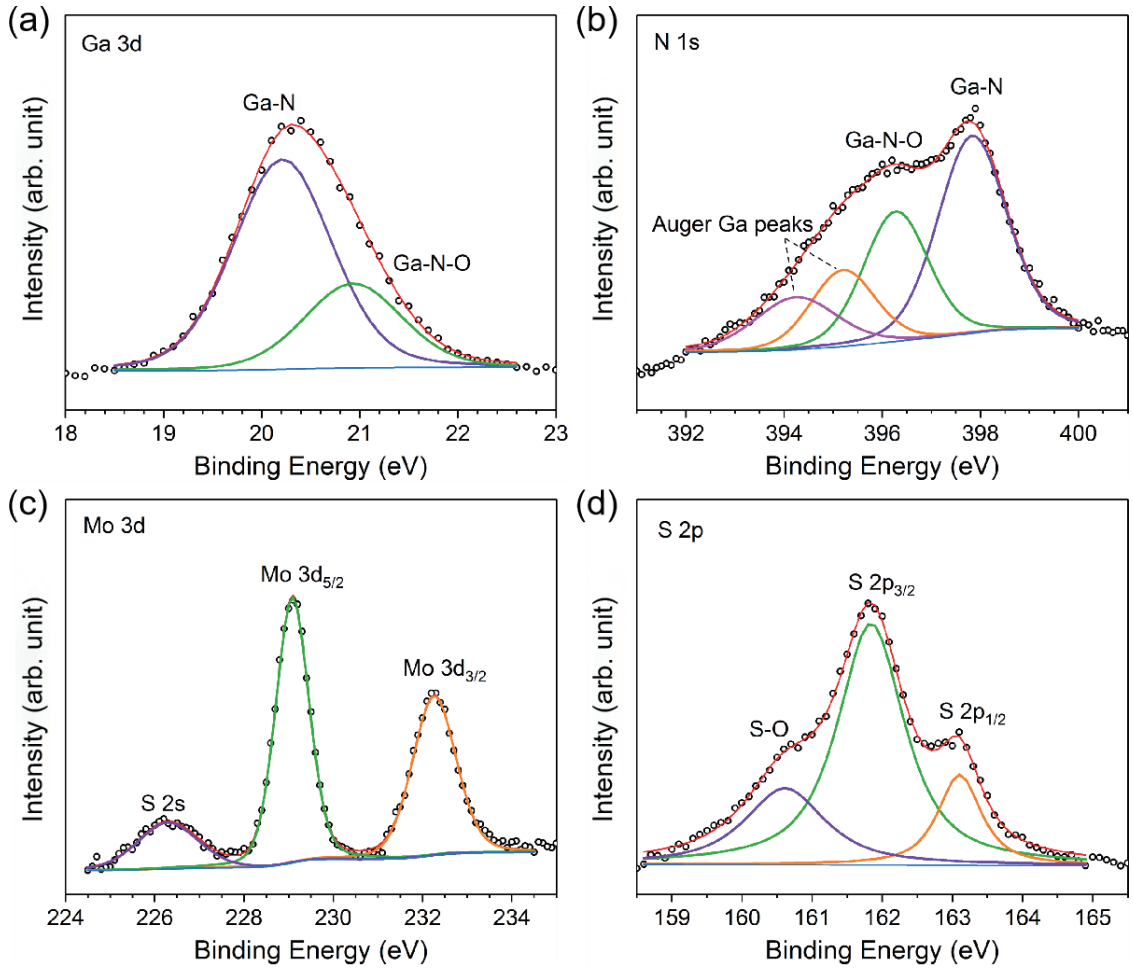

Fig. 6. (Color online) XPS core-level spectra of (a) Ga 3d, (b) N 1s, (c) Mo 3d, and (d) S 2p of the GM-500 electrode.

conversely, the discharging process. The high surface area of the GaN NWs provides the surface oxidation and redox reaction sites, which leads to the Faradaic capacity of the GaN electrodes. It can be seen from the Mo 3d XPS scan spectrum in Fig. 6(c) that two strong peaks at 229.1 and 232.3 eV are the characteristic binding energies of Mo $3d_{5/2}$ and Mo $3d_{3/2}$, respectively.[36] The weak peak at 226.3 eV belongs to the S 2s energy level. The binding energies of S $2p_{3/2}$ (161.8 eV) and S $2p_{1/2}$ (163.1) in Fig. 6(d) are ascribed to the Mo-S bond. A chemical state of S-O bonding that appeared at 160.6 eV is from the residual electrolyte.[37] Charge storage in MoS2 NSs may be realized by a non-Faraday process involving the surface adsorption of protons or cations and Faraday charges. From the CV and GCD curves, the enhanced capacity of the GaN–MoS_2 composite electrode can be ascribed to the H^+ ions absorbed on the MoS_2 surface and intercalated into the near-surface layer of MoS_2. Thus, a possible Faradaic dominated mechanism is the intercalation and deintercalation of H^+ in the MoS_2 NSs during reduction and oxidation.[38]

$$MoS_2 + xH^+ + xe^- \leftrightarrow MoS - SH_x \tag{3}$$

The high density of edges in the MoS_2 NSs provides a large number of active sites for the redox reaction. To summarize, the Faradaic charging dominates the charge storage of the GM-500 electrode. The large surface area of the GaN–MoS_2 composite NWs and the numerous active sites of MoS_2 NSs benefit the capacity, which resulted in the enhancement of the capacity of the GaN–MoS_2 composite electrode.

4. Conclusion

The GaN NWs coated with MoS_2 NSs on graphite paper have been successfully prepared by chemical vapor deposition. The electrochemical performance characteristics of GaN and GaN–MoS_2 composite NW electrodes exhibit battery-type features. The optimal MoS_2-coated GaN composite electrode shows a specific capacity of 173.4 mC cm^{-2} at 1 mA cm^{-2}, which is greater than that of GaN NWs (128.8 mC cm^{-2}). The enhancement of electrochemical performance was attributed to the synergistic effect of high specific surface area and effective ion diffusion channels resulting from the coupling of MoS_2 NSs with GaN NWs. In this work, we demonstrate the promising application of GaN–MoS_2 composite NWs as highly effective electrode materials for energy storage.

Acknowledgments

This work was supported by the Natural Science Foundation of China (51572092).

References

1 B. E. Conway: J. Electrochem. Soc. **138** (1991) 1539. https://doi.org/10.1149/1.2085829
2 Z. Yu, L. Tetard, L. Zhai, and J. Thomas: Energy Environ. Sci. **8** (2015) 702. https://doi.org/10.1039/C4EE03229B
3 Y. Gogotsi and R. M. Penner: ACS Nano **12** (2018) 2081. https://doi.org/10.1021/acsnano.8b01914
4 P. Simon and Y. Gogotsi: Nat. Mater. **7** (2008) 845. https://doi.org/10.1038/nmat2297
5 T. Brousse, D. Bélanger, and J. W. Long: J. Electrochem. Soc. **162** (2015) A5185. https://doi.org/10.1149/2.0201505jes
6 L. L. Zhang and X. S. Zhao: Soc. Rev. **38** (2009) 2520. https://doi.org/10.1039/B813846J
7 J. Jiang, Y. Li, J. Liu, X. Huang, C. Yuan, and W. Lou Xiong: Adv. Mater. **24** (2012) 5166. https://doi.org/10.1002/adma.201202146
8 Y. Shi, L. Peng, Y. Ding, Y. Zhao, and G. Yu: Chem. Soc. Rev. **44** (2015) 6684. https://doi.org/10.1039/C5CS00362H
9 P. Yang, D. Chao, C. Zhu, X. Xia, Y. Zhang, X. Wang, P. Sun, B. K. Tay, Z. X. Shen, W. Mai, and H. J. Fan: Adv. Sci. **3** (2015) 1500299. https://doi.org/10.1002/advs.201500299
10 H. Cui, G. Zhu, X. Liu, F. Liu, Y. Xie, C. Yang, T. Lin, H. Gu, and F. Huang: Adv. Sci. **2** (2015) 1500126. https://doi.org/10.1002/advs.201500126
11 B. Wei, H. Liang, D. Zhang, Z. Wu, Z. Qi, and Z. Wang: J. Mater. Chem. A **5** (2017) 2844. https://doi.org/10.1039/C6TA09985H
12 S. Chattopadhyay, A. Ganguly, K. H. Chen, and L. C. Chen: Crit. Rev. Solid State Mater. Sci. **34** (2009) 224. https://doi.org/10.1080/10408430903352082
13 S. Wang, L. Zhang, C. Sun, Y. Shao, Y. Wu, J. Lv, and X. Hao: Adv. Mater. **28** (2016) 3768. https://doi.org/10.1002/adma.201600725
14 S. Wang, C. Sun, Y. Shao, Y. Wu, L. Zhang, and X. Hao: Small **13** (2017) 1603330. https://doi.org/10.1002/smll.201603330
15 C. Sun, M. Yang, T. Wang, Y. Shao, Y. Wu, and X. Hao: ACS Appl. Mater. Interfaces **10** (2018) 2574. https://doi.org/10.1021/acsami.7b16416

16 X. Zhao, B. M. Sánchez, P. J. Dobson, and P. S. Grant: Nanoscale **3** (2011) 839. https://doi.org/10.1039/C0NR00594K
17 S. Wang, Y. Shao, W. Liu, Y. Z. Wu, and X. Hao: J. Mater. Chem. A **6** (2018) 13215. https://doi.org/10.1039/C8TA04182B
18 C. Sun, M. Yang, T. Wang, Y. Shao, Y. Wu, and X. Hao: ACS Appl. Mater. Interfaces **9** (2017) 26631. https://doi.org/10.1021/acsami.7b07277
19 E. G. da Silveira Firmiano, A. C. Rabelo, C. J. Dalmaschio, A. N. Pinheiro, E. C. Pereira, W. H. Schreiner, and E. R. Leite: Adv. Energy Mater. **4** (2014) 1301380. https://doi.org/10.1002/aenm.201301380
20 L. Ma, L. M. Xu, X. P. Zhou, and X. Y. Xu: Mater. Lett. **132** (2014) 291. https://doi.org/10.1016/j.matlet.2014.06.108
21 H. Li, Y. Zhao, and C.-A. Wang: J. Mater. Sci.: Mater. Electron. **29** (2018) 13703. https://doi.org/10.1007/s10854-018-9499-9
22 B. D. Falola, T. Wiltowski, and I. I. Suni: J. Electrochem. Soc. **163** (2016) D568. https://doi.org/10.1149/2.0011610jes
23 T. N. Y. Khawula, K. Raju, P. J. Franklyn, I. Sigalas, and K. I. Ozoemena: J. Electrochem. Soc. **163** (2016) A1927. https://doi.org/10.1149/2.0601609jes
24 Z. Xu, K. Yao, Z. Li, L. Fu, H. Fu, J. Li, L. Cao, and J. Huang: J. Mater. Chem. A **6** (2018) 10535. https://doi.org/10.1039/C8TA02339E
25 T. Wang, F. Chen, X. Ji, and Q. Zhang: Superlattices Microstruct. **119** (2018) 114. https://doi.org/10.1016/j.spmi.2018.04.047
26 F. Chen, T. Wang, L. Wang, X. Ji, and Q. Zhang: J. Mater. Chem. C **5** (2017) 10225. https://doi.org/10.1039/c7tc03231e
27 T. Azuhata, T. Sota, K. Suzuki, and S. Nakamura: J. Phys.: Condens. Matter **7** (1995) L129. https://doi.org/10.1088/0953-8984/7/10/002
28 H. L. Liu, C. C. Chen, C. T. Chia, C. C. Yeh, C. H. Chen, M. Y. Yu, S. Keller, and S. P. DenBaars: Chem. Phys. Lett. **345** (2001) 245. https://doi.org/10.1016/S0009-2614(01)00858-2
29 C. Lee, H. Yan, L. E. Brus, T. F. Heinz, J. Hone, and S. Ryu: ACS Nano **4** (2010) 2695. https://doi.org/10.1021/nn1003937
30 S. D. Wolter, B. P. Luther, D. L. Waltemyer, C. Önneby, S. E. Mohney, and R. J. Molnar: Appl. Phys. Lett. **70** (1997) 2156. https://doi.org/10.1063/1.118944
31 C. Ozgit-Akgun, F. Kayaci, S. Vempati, A. Haider, A. Celebioglu, E. Goldenberg, S. Kizir, T. Uyar, and N. Biyikli: J. Mater. Chem. C **3** (2015) 5199. https://doi.org/10.1039/C5TC00343A
32 G. Moldovan, I. Harrison, M. Roe, and P. D. Brown: Inst. Phys. Conf. Ser. **179** (2004) 115. https://core.ac.uk/outputs/17855/
33 D. Choi, G. E. Blomgren, and P. N. Kumta: Adv. Mater. **18** (2006) 1178. https://doi.org/10.1002/adma.200502471
34 B. Avasarala and P. Haldar: Electrochimica Acta **55** (2010) 9024. https://doi.org/10.1016/j.electacta.2010.08.035
35 A. Achour, J. B. Ducros, R. L. Porto, M. Boujtita, E. Gautron, L. Le Brizoual, M. A. Djouadi, and T. Brousse: Nano Energy **7** (2014) 104. https://doi.org/10.1016/j.nanoen.2014.04.008
36 R. K. Chava, J. Y. Do, and M. Kang: ACS Sustainable Chem. Eng. **6** (2018) 6445. https://doi.org/10.1021/acssuschemeng.8b00249
37 N. D. Chuong, T. D. Thanh, N. H. Kim, and J. H. Lee: ACS Appl. Mater. Interfaces **10** (2018) 24523. https://doi.org/10.1021/acsami.8b06485
38 J. M. Soon and K. P. Loh: Electrochem. Solid-State Lett. **10** (2007) A250. https://doi.org/10.1149/1.2778851